Low viscosity, high concentration pyridinium anolytes for organic non-aqueous redox flow batteries

*Sharmila Samaroo[1], Annabelle L. Pattillo[1], Dominik Servinski[1], William R. Kruper[3], Davarius D. Carter[3], Thomas F. Guarr[2,3], David P. Hickey[1]**

[1]Department of Chemical Engineering and Materials Science, Michigan State University; East Lansing, MI 48824, USA.

[2]Michigan State University Bioeconomy Institute, Michigan State University; Holland, MI, 49424, USA.

[3]Jolt Energy Storage Technologies, LLC; Holland, MI 49424 USA.

KEYWORDS: Structure-property relationships, redox-active organic molecule, electrolyte, energy storage, physicochemical properties, conductivity, CH-π interactions

ABSTRACT:

The ability to tune various physicochemical and electrochemical properties of redox-active organic molecules (ROMs) independently from one-another has been a long-standing goal of researchers attempting to design active materials for redox flow batteries (RFBs). While

increasing ROM solubility is essential for improving energy densities, power densities, and lowering costs of RFBs, the use of elevated ROM concentrations in an RFB often causes solution properties – such as viscosity and conductivity – to vary in unpredictable and impactful ways. At elevated concentration, strong electrostatic interactions between ROMs, solvent, and supporting electrolyte often result in high viscosity and low solution conductivity, both of which are deleterious to practical RFB operation. Recently, it has been demonstrated that a class of 2,6-dimethylpyridinium-derived ROMs can achieve a broad range of solubilities in acetonitrile by fine-tuning unique intermolecular CH-π interactions, which disrupt electrostatic solute-solute interactions. Here, we evaluate the electrochemical characteristics for a library of 23 N-substituted 4-aryl-2,6-dimethylpyridinium ROMs and measure solution viscosities and conductivities at variable concentrations for three representative species in acetonitrile. We show that this class of 2,6-dimethylpyridinium ROMs demonstrate low reduction potentials and rapid diffusion coefficients at low concentrations, and we find that representative pyridinium ROMs exhibit low dynamic viscosities (~1 cP), and high conductivities (25.0 - 32.8 mS cm^{-1}) at elevated concentrations in acetonitrile. Our results suggest that trends in solution viscosity may be a consequence of distinct intermolecular interactions prevalent among pyridinium molecules and these desirable qualities further establish pyridiniums as a promising anolyte for emerging grid-scale energy storage technologies.

INTRODUCTION

Redox flow batteries (RFBs) are an attractive form of large-scale energy storage that may aid in integrating the growing number of renewable energy resources into the existing electrical grid. RFBs store energy in the form of solvated redox-active molecules by interconverting

electrical and chemical energy through electrochemical redox reactions.[1–4] One subset of RFBs, non-aqueous redox flow batteries (NRFBs), are particularly attractive because of their wide electrochemical stability window (up to 4 V) and because they enable the utilization of cost-effective and modular redox-active organic molecules (ROMs).[5,6] While many promising ROMs are sparingly soluble in water, they exhibit substantially higher solubility in polar aprotic solvents, such as acetonitrile and propylene carbonate. This improved solubility is important, because NRFB energy storage capacity is directly proportional to ROM concentration. Despite the recent advancements in identifying and developing numerous classes of ROMs that exhibit promising electrochemical stability and low reduction potentials (or high oxidation potentials), many suffer from high dynamic viscosity (> 10 cP) and low conductivity (< 5 mS cm^{-1}) at concentrations that would be sufficiently high for practical operation (> 0.5 M).[7,8] In the context of an NRFB, highly viscous ROM solutions limit flow rates and cause pressure drop across the flow field (both of which limit mass transport, and thus limit charge/discharge rates), while poorly conductive solutions result in high overpotentials and low storage efficiency.[9,10] Therefore, there remains a need to identify classes of ROMs demonstrating moderate viscosities and conductivities at elevated concentrations.

A unique correlation was recently reported between intermolecular solute-solute interactions and the maximum solubility for a class of 2,6-dimethyl-4-arylpyridinium ROMs in polar aprotic solvents.[11] Specifically, intermolecular interactions between CH groups and π-electrons of neighboring pyridinium ROMs were shown to disrupt the formation of stable ionic lattices. As a result, the propensity for a particular pyridinium ROM to participate in CH-π interactions is proportional to its solubility in acetonitrile, propylene carbonate, cyclohexanone, and THF.[11] Conventional molecular engineering-centered strategies to improve ROM solubility

involve tuning a parent structure to either promote electrostatic solute-solvent interactions (i.e., adding a polyethylene glycol, PEG, chain or a charged functional group)[12,13] or increase solvent-accessible surface area (e.g., by adding a flexible alkyl pendant group).[14–16] Both of these strategies can increase the maximum solubility of a parent ROM but require the incorporation of a large molecular substituent. Unfortunately, substantial increases in molecular weight of the ROM solute are often accompanied by increased viscosity at high concentrations. By contrast, promotion of CH-π interactions (and, thus, increased solubility) can be accomplished with minimal modification to the parent pyridinium ROM structure (as illustrated in Figure 1). Consequently, we considered the possibility that this unique method of enhancing pyridinium ROM solubility may break the conventional solubility/viscosity paradigm, which suggests RFB solutions with sufficiently high concentration of active material will suffer from high viscosity. Herein, we present a study on the impact of ROM concentration on viscosity and conductivity for a series of 4-aryl-2,6-dimethylpyridinium salts in acetonitrile.

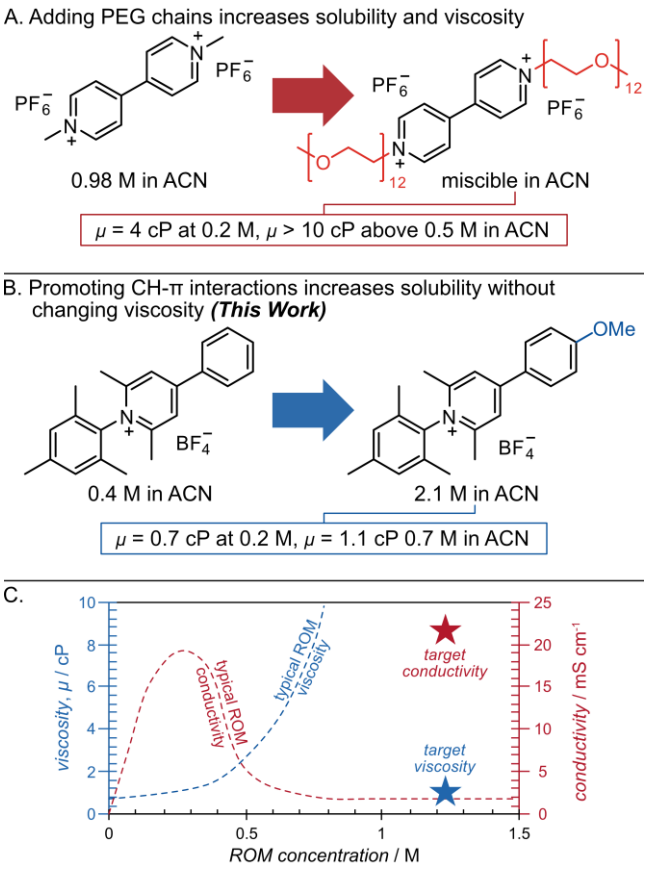

Figure 1. Comparison of strategies used to increase ROM solubilities and the resulting viscosity and conductivity trends. (A) An example of a conventional strategy (i.e., adding PEG chains) used to increase viologen [12,13]ROM solubility.[17](REF) (B) An alternative approach promoting CH-π interactions in pyridinium[11] ROMs (bottom) with their respective viscosities and conductivities at increasing concentrations in acetonitrile. (C) Ideal ROMs have low dynamic viscosity (< 10 cP) and high conductivity (> 5 mS cm^{-1}) at elevated concentrations (> 0.5 M).[7,8]

Viscosity is a fundamental property of NRFB solutions that is complex and critical for dictating the economic viability of any proposed flow battery. Highly viscous electrolyte solutions require higher energy demand to pump the active NRFB fluid through a porous electrode during charging and discharging. Consequently, solution viscosity is a significant factor for determining performance and operating costs.[18,19] In addition to cost, highly viscous RFB solutions are intrinsically linked to performance limitations, as shown by the Stokes-Einstein equation,

(1) $$D = \frac{k_B T}{\alpha \pi \mu d}$$

where D is solute diffusivity, k_B is the Boltzmann constant, T is absolute temperature, α is a coefficient that arises from the boundary conditions of the solute-solvent interface (where α ranges from 4 for no-slip to 6 for slip conditions), μ is the dynamic viscosity, and d is the molecular diameter.[20] Viscosity of NRFB solutions is inversely proportional to ROM diffusivity as well as solution conductivity, both of which are critical for achieving high power densities.[10,21] Recent works have explored the effect of varying either ROM or supporting electrolyte salt concentrations in non-aqueous systems on the properties, such as ionic conductivity and viscosity, of the corresponding electrolyte solution.[7,9,10,22] While ionic conductivity gradually decreases with increasing concentration for non-ionic ROMs, for ionic ROMs and supporting electrolyte, the relationship between concentration and ionic conductivity is parabolic, increasing at low concentration but decreases after reaching a maximum value.[23] The dependence of viscosity on solute concentration is proportionally similar for both ionic and nonionic solutes; as concentration increases, viscosity increases asymptotically. Therefore, it is desirable to identify molecular design strategies to increase both the concentration of maximum conductivity and the onset of exponential increase in viscosity with concentration.

Identifying structure-property relationships in ROMs is complicated by the often-limited ability to systematically vary steric and electronic influence of a parent ROM's substituents. Recently, we reported a modular synthetic procedure to prepare a diverse library of N-substituted 4-aryl-2,6-dimethylpyridinium derivatives.[11] These ROMs provide a modular, rigid core structure that is ideal for probing structure-property relationships. Furthermore, they are promising anolyte candidates, exhibiting exceptionally low reduction potentials, persistence in the radical state, and high solubility in multiple polar aprotic solvents. Herein, we assess the electrochemical characteristics of this uniquely modular class of pyridinium ROMs and evaluate the viscosity and

ionic conductivity as a function of concentration for a representative selection of molecules. Diffusion coefficients are measured by cyclic voltammetry for each pyridinium derivative in acetonitrile to provide insight into solute-solvent interactions. Additionally, solution viscosities and conductivities of a representative selection of pyridiniums in acetonitrile are measured at variable concentrations to determine the impact of CH-π interactions on these critical physicochemical properties as ROMs approach their solubility limits in acetonitrile.

EXPERIMENTAL METHODS

Materials

All synthetic starting materials, including 2,6-dimethyl-γ-pyrone (Ambeed), Grignard reagents (Alfa Aesar or Sigma-Aldrich), and all amines (various sources) were of the highest purity available and used as received. Arylmagnesium bromides were purchased as 1 M solutions in THF from Sigma-Aldrich or Thermo Scientific. Anhydrous tetrabutylammonium hexafluorophosphate (99.8%) was purchased from MilliporeSigma. The acetonitrile used during electrochemical evaluation was purchased from Acros Organics (99.9%, Extra Dry over Molecular Sieve, AcroSeal) and the acetonitrile used to make conductivity and viscosity solutions was purchased from Oakwood Chemical (HPLC grade).

General Synthesis of 2,6-Dimethylpyridiniums

All pyrylium intermediates were synthesized following a modified procedure reported by DiMauro and Kozlowski[24,25] and all pyridiniums were synthesized using procedures previously reported by Samaroo *et al*.[26]

Synthesis of 2,6-Dimethylpyrylium Intermediate

In an oven-dried 250 mL round bottom flask, 2,6-dimethyl-γ-pyrone (27 – 34 mmol) was dissolved in THF (120 – 140 mL) under nitrogen and cooled to 5 °C in an ice bath. One equivalent of aryl magnesium bromide (in a 1 M solution with THF) was added dropwise to the stirring solution. After the addition, the reaction mixture warmed to room temperature over an hour. Boron trifluoride diethyl etherate solution was added to the stirring reaction mixture, yielding a precipitate that was isolated by filtration and washed with diethyl ether. The intermediate pyrylium product was purified by recrystallization in a 1:1 water/methanol mixture (yields ranged from 40% to 48%).

Synthesis of 2,6-Dimethylpyridinium

The desired pyridinium derivatives were generated by reacting the respective pyrylium intermediate with a primary amine. In a 50 mL round bottom flask equipped with a magnetic stir bar and condenser, 4-substituted 2,6-dimethyl-pyrylium tetrafluoroborate (9 – 18 mmol) was suspended in ethanol. Approximately 1.2 equivalents of the corresponding primary amine were added, and the mixture was refluxed for 4 hours under flowing nitrogen. The solution was cooled to room temperature overnight and diluted with diethyl ether. The precipitate was isolated by filtration and dried under vacuum to afford a solid product (yields ranged from 45% to 68%).

Cyclic Voltammetry

Cyclic voltammograms (CVs) of all pyridinium derivatives were measured in a nitrogen atmosphere glovebox using a Metrohm MultiAutolab M204 Potentiostat. Solutions used for electrochemical experiments contained 1 mM pyridinium, 1 mM ferrocene as an internal reference, and 100 mM tetrabutylammonium hexafluorophosphate in acetonitrile (99%, Extra Dry)

as the supporting electrolyte. Experiments were performed using 3 mm glassy carbon working electrode and a non-aqueous Ag/Ag^+ reference electrode (10 mM $AgNO_3$ in acetonitrile) at 22 °C.

For reversibility assessments, CVs were collected at a scan rate of 200 mV s^{-1}. The anodic peak current (i_{pa}) was divided by the cathodic peak current (i_{pc}) to yield the peak height ratio, and the potentials at peak anodic current (E_{ipa}) and cathodic current (E_{ipc}) were used to measure peak-to-peak separations.

For determination of diffusion coefficients, CVs were performed at scan rates of 20, 50, 100, 200, 400, 800, 1200, and 1600 mV s^{-1}. Peak currents (anodic and cathodic, i_{pa} and i_{pc} respectively) were plotted vs the square root of the corresponding scan rate (mV s^{-1}) to give a linear trend consistent with the Randles-Sevcik equation to determine diffusion coefficients of each derivative. A detailed description of diffusion coefficient calculation can be found in the Supporting Information.[27]

Viscosity

Kinematic viscosities for solutions of compounds **3**, **5**, and **17** were evaluated at variable concentrations in pure acetonitrile using a calibrated Ubbelohde viscometer (Cannon, Size 0). Concentration ranges were selected based on the maximum solubility in acetonitrile; 0.29, 0.15, 0.07, 0.04, and 0.02 mM for **3**; 0.32, 0.16, 0.08, 0.04, and 0.02 mM for **5**; 0.68, 0.34, 0.17, 0.09, and 0.04 mM for **17.** Solutions were made by saturating acetonitrile (HPLC grade) with each compound at ambient temperatures in a graduated cylinder, then adding 3-5 mL of pure acetonitrile (to avoid precipitation in the highest concentration solutions occurring with slight temperature fluctuations). The initial solution was diluted by half with pure acetonitrile, and subsequent serial dilutions were prepared for a total of five concentrations for viscosity measurements. The viscosity

of pure deionized water and pure acetonitrile were measured in the same viscometer to confirm calibration ranges and establish viscosities at ambient temperature. Ambient temperature was recorded at the start of each measurement (19.5 °C ± 0.4 °C). Reported values include the average of five consecutive measurements and their standard deviations.

The density of each solution was measured to calculate dynamic viscosity from the corresponding kinematic viscosity. Densities were measured by weighing 100 μL of each solution at ambient temperature. Dynamic viscosities were calculated by dividing the measured kinematic viscosity by the corresponding density for each solution.

Conductivity

Solution conductivities of compounds **3**, **5**, and **17** were evaluated at variable concentrations in acetonitrile using an Orion Star A212 Conductivity Meter (ThermoScientific). Solutions of each representative pyridinium were prepared as described above for viscosity measurements. The conductivity of pure deionized water and pure acetonitrile (HPLC grade) were measured to establish conductivities at ambient temperature. Ambient temperature was recorded at the start of each measurement (17.7 °C ± 0.5 °C). Reported values include the average of three consecutive measurements and their standard deviations.

RESULTS & DISCUSSION

For this study, we prepared a library of 23 structural derivatives of N-substituted 4-aryl-2,6-dimethylpyridinium tetrafluoroborate salts using a modular synthetic approach as described previously. Pyridiniums were derivatized by either varying the N-substituent or modifying the 4-aryl ring, and the library was selected to contain sufficient steric and electronic variation at both

positions to elucidate broader structure-property relationships for this class of pyridinium ROMs. Variation of the 4-aryl ring was limited to either all hydrogen (i.e., the parent unmodified phenyl ring) (**1**, **3**, **4**, **5**, **7**, **18**), 4-methyl (**2**, **8**, **9**, **10**, **11**, **13**, **15**, **21**, **22**), 2,4-dimethyl (**12**, **19**, **20**), or 4-methoxy (**6**, **14**, **16**, **17**, **23**) substituents; however, variation of the N-substituent represents a wider range of functionality, including flexible butyl or oligoether chains, and sterically hindering aryl rings with either electron donating or withdrawing substituents. The breadth of substituent variations spanning across all 23 compounds is particularly valuable in revealing the less predictable, combined effects of electron density and sterics in the 4-position and N-position.

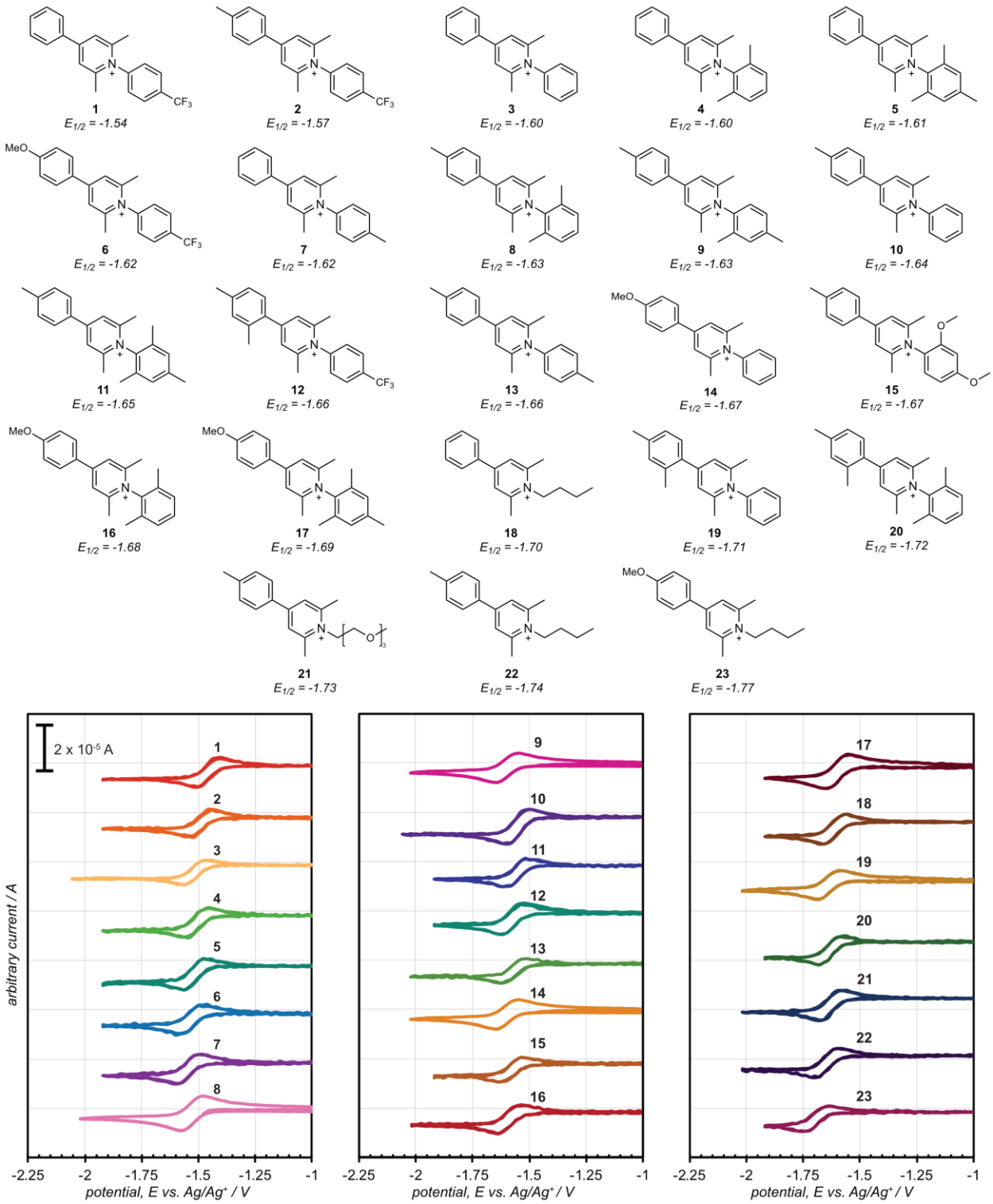

Figure 2. Summary of molecular structures and representative cyclic voltammograms. (Top) Structure and corresponding reversible redox potential (V vs. Fc/Fc^{+}) for all 23 pyridinium ROMs studied. (Bottom) Representative cyclic voltammograms (CVs) for each pyridinium ROM (1 mM active species) in acetonitrile. Experiments were performed using 3 mm GCE working electrode

and Ag/Ag^+ reference electrode with 100 mM tetrabutylammonium hexafluorophosphate in acetonitrile as the supporting electrolyte at 22 °C and 200 mV s^{-1} under N_2 atmosphere.

Electrochemistry

To initiate our investigation, we first measured standard electrochemical properties of each pyridinium using cyclic voltammetry (CV) as shown in Figure 2. Redox potentials of the series of 23 compounds evaluated spans from -1.54 to -1.77 V vs. ferrocene, and CVs reveal that every derivative exhibit good electrochemical reversibility (*i.e.*, peak current ratio = 1 and peak-to-peak separation less than ~100 mV). It should be noted that compounds are numbered by decreasing redox potential, thus compound **1** has the most positive reduction potential and compound **23** has the most negative reduction potential. For anolyte ROMs, such as pyridiniums, more negative reduction potentials are desirable because both energy and power densities are dependent on the difference in catholyte oxidation potential and anolyte reduction potential. It is commonly understood that the electronic nature of substituents on a parent ROM influences the corresponding reduction potential.[4,28,29] Electron withdrawing groups pull electron density away from the core structure, making reduction easier (thus resulting in more positive redox potentials), while electron donating groups have the opposite effect, making reduction more difficult (thus resulting in lower redox potentials).

The influence of substituent electronics on redox potential can be observed across the library of pyridiniums. We can see these effects of certain substituents demonstrated across this library of molecules. Compounds **1** and **2** contain electron-withdrawing trifluoromethylphenyl N-substituents and exhibit the most positive redox potentials, while **22** and **23** contain electron-donating aliphatic chains as N-substituents and exhibit the most negative redox potentials in the library. Pyridinium redox potentials generally follow a Hammett relationship, in which redox potential is directly proportional to the sum of Hammett substituent constants (σ_p) for groups on

the N- and 4-position of the parent 2,6-dimethylpyridinium ring.[30] This trend is illustrated in Figure 3; however, there are three notable (**12**, **19**, **20**) outliers that all contain 2,4-dimethylphenyl groups as the 4-substiuent. The presence of a 2-methyl group on the 4-aryl substituent introduces enough steric hindrance to cause the 4-aryl ring to deviate from the pyridinium plane, thereby disrupting the overlap between the p-orbitals of the two rings. This disruption alters the inductive influence of the 4-aryl ring on the redox-active pyridinium ring and may account for the deviation from pure Hammett behavior. Taken together, these trends provide insights towards which functional groups may produce desirable properties in future iterations of pyridinium molecules. In addition to redox potentials, CV data was used to extract diffusivities for pyridinium ROMs in our library.

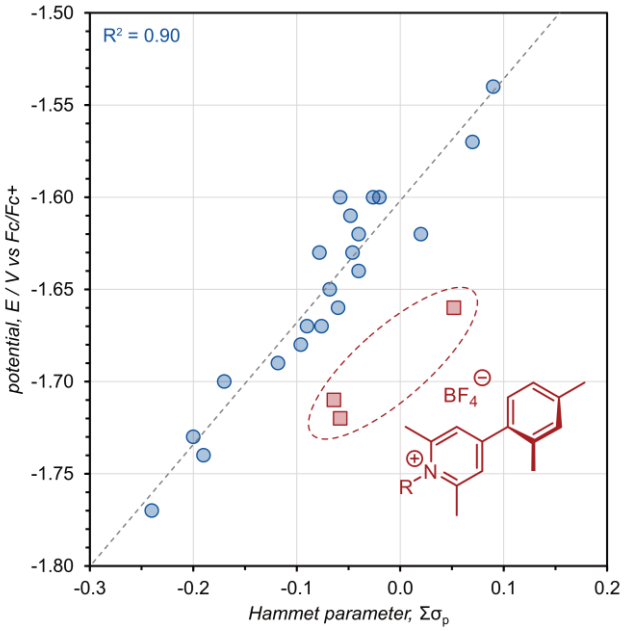

Figure 3. Redox potential of pyridinium ROMs follows a Hammett relationship. Reversible redox potential for all 23 pyridinium ROMs vs. the sum of Hammett σ_p parameters for the 4- and N-substituents.[30] Pyridiniums with 4-phenyl, 4-(*p*-methoxyphenyl), and 4-(*p*-methylphenyl) substituents (blue circles) correlate strongly to the sum of Hammett parameters, whereas pyridiniums with 4-(2,4-dimethylphenyl) (red squares) are notable outliers.

Diffusion coefficients (or diffusivities) are commonly measured as an initial assessment of electrode kinetics and provide critical information about how ROMs behave in solution. The

diffusion coefficients for the oxidized and reduced forms of all 23 compounds were determined by collecting cyclic voltammograms (CVs) at variable scan rates and applying the Randles-Sevcik relationship.[27] For the pyridiniums studied, most exhibited diffusion coefficients that range from 3 x 10^{-6} cm^2 s^{-1} and 9 x 10^{-6} cm^2 s^{-1}; however, the most rapid diffusion coefficients of D = 1.9 x 10^{-5} cm^2 s^{-1} and D = 1.4 x 10^{-5} cm^2 s^{-1} for the oxidized forms of **3** and **10** respectively, were approximately twice as fast. For dilute solutions in which solution viscosity is the same for all pyridiniums, the Stokes-Einstein (SE) equation (Equation 1) suggests that diffusivity should change linearly with the Stokes radius. A plot of diffusion coefficients measured by CV for all 23 pyridiniums versus the diffusion coefficient calculated from the SE equation (using the molecular radii extracted from previously published crystal structures of each pyridinium, details provided in the Supporting Information) is shown in Figure 4. The SE equation generally provides an accurate estimate of the measured diffusion coefficient based on the crystal lattice-derived molecular radius (where small deviations are within experimental error); however, it significantly underpredicts the diffusivities of **3** and **10** which are significantly faster despite having a similar molecular radius to the other measured pyridiniums.

One possible explanation for this faster than expected diffusivity may be related to the interaction between **3** or **10** with the surrounding solvent. The α term in the SE equation describes the friction between the solute and surrounding solvent, where $\alpha = 6$ is used for no-slip conditions (i.e., strong solvent-solute friction) and $\alpha = 4$ is used for slip conditions (i.e., weak or no solvent-solute friction).[20] For most dilute electrolyte solutions, no-slip conditions ($\alpha = 6$) provide an accurate estimate of diffusivity. If we assume that **3** and **10** interact more weakly with the solvent (i.e., allow $\alpha = 4$), then their predicted diffusivities are more closely aligned with the measured values. While this interpretation is highly speculative and requires further experimental

investigation, the observation suggests that this class of pyridiniums exhibits physicochemical behavior which deviates from that predicted using simple molecular descriptors (e.g., Stokes radius).

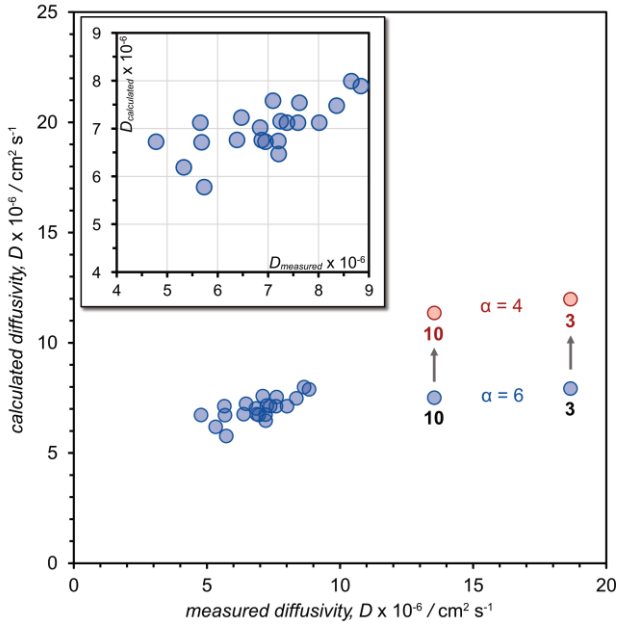

Figure 4. Diffusion coefficients measured by CV vs calculated from Stoke-Einstein for pyridiniums in acetonitrile. Calculated diffusion coefficients were determined from the Stokes-Einstein equation[20] based on the crystal structure-derived radius and using either the coefficient, $\alpha = 6$ (blue circles) assuming the no-slip condition, or $\alpha = 4$ (red circles) assuming slip conditions. Measured diffusion coefficients were determined from CVs at variable scan rates and applying the Randles-Sevcik relationship.[27] Experiments were performed using 3 mm GCE working electrode and Ag/Ag^+ reference electrode with 1 mM pyridinium and 100 mM tetrabutylammonium hexafluorophosphate in acetonitrile as the supporting electrolyte at 22 °C under a N_2 atmosphere.

Viscosity

Pyridinium-based ionic liquids have been of previous interest for a variety of industrial applications, and some studies have explored how viscosity is influenced by varied substitution, aliphatic chain length, and counterions for simple pyridinium ionic liquids.[31–33] Changes in viscosity from these studies has been rationalized by effects of hydrogen bonding and Van der Waals interactions; however, efforts to predict these behaviors is limited. Furthermore, many structure-viscosity correlations suggest that the incorporation of flexible aliphatic chains or

oligoether chains (often used to improve ROM solubility) strongly correlates to substantially increased viscosity at concentrations approaching or exceeding 1 M in polar aprotic solvents.[16,17] Our recent work demonstrated the ability to achieve high ROM solubility without long, flexible substituents by exploiting intermolecular CH-π interactions. Based on this, we hypothesized that pyridiniums known to exhibit CH-π associations may not suffer from similar increases in viscosity at high concentrations.

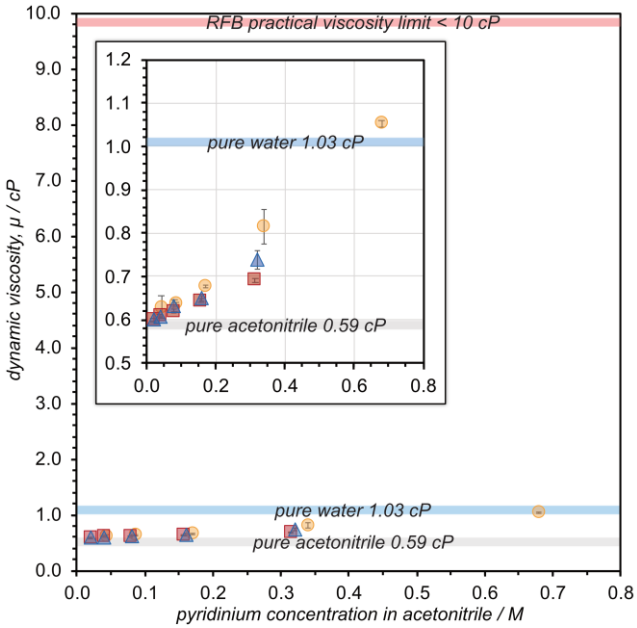

Figure 5. Concentration dependent dynamic viscosities in acetonitrile of compound **3** (blue triangles), **5** (red squares), and **17** (yellow circles) pyridiniums. Reported viscosity values represent the average of $n = 5$ replicates, and the error bars represent the respective standard deviations at (19.5 °C ± 0.4 °C).

To test this hypothesis, we selected three pyridiniums previously determined to participate in varying amounts of CH-π bonding and evaluated their kinetic viscosity at variable concentrations in acetonitrile.[11] Compounds **3**, **5**, and **17** were selected for their incremental structural variation with 4- and N-substituents as 4-phenyl/N-phenyl, 4-phenyl/N-mesityl, or 4-*p*-methoxyphenyl/N-mesityl, respectively. Additionally, **3**, **5**, and **17** were previously shown to exhibit either limited (**3**, **5**) or extensive (**17**) CH-π solute-solute interactions.

A plot of dynamic viscosity vs pyridinium concentration is shown in Figure 5 and reveals a positive linear relationship between viscosity and concentration as each pyridinium nears their respective solubility limits in acetonitrile. This general trend is consistent with previously reported ROMs in polar aprotic solvents; however, the magnitude of their dynamic viscosities was found to be exceptionally low. The resulting dynamic viscosities for all three derivatives nearing their maximum solubility (in acetonitrile at 19.5 °C ± 0.4 °C) were measured as 0.691 ± 0.005 cP (at 0.3 M for **3**), 0.74 ± 0.02 cP (at 0.3 M for **5**), and 1.052 ± 0.008 cP (at 0.7 M for **17**). For comparison, many NRFB ROM solutions suffer from dynamic viscosities exceeding 10 cP at 0.5 M in comparable solvents.[7,8] Additionally, the dynamic viscosities of pyridinium solutions were all measured to be near or lower than that of pure water, which was measured to be 1.00 cP with the same experimental procedure and conditions. While there was no observed correlation between viscosity and CH-π interactions for the set of compounds (and experimental conditions) tested, the low viscosities in acetonitrile highlight the promise of this class of pyridinium ROMs for NRFB applications.

Conductivities

Another critical property for NRFB ROMs, ionic conductivity, is inversely impacted by increasing viscosity; so that with incremental increases in viscosity in acetonitrile, one would expect reduced diffusivities and subsequently diminishing conductivities (consistent with the Stokes-Einstein equation and the Nernst-Stokes relationship).[10,19,21] At low concentrations of ionic ROMs in pure acetonitrile, increased viscosity is generally negligible and conductivity increases; however, as ROM concentrations generally approach ~0.4 M, increasing viscosity (and thus, decreasing ROM diffusivity) is sufficient to diminish the solutions ionic conductivity.[23]

Consequently, large amounts of supporting electrolyte are necessary to maintain sufficiently high conductivity for practical operation of NRFBs.

To determine whether similar trends would be observed for 2,6-dimethyl pyridinium salts, ionic conductivities were measured for solutions of **3**, **5**, and **17** in pure acetonitrile at varying concentrations. The resulting plots of pyridinium concentration versus ionic conductivity (shown in Figure 6) reveal expected increases in conductivity with ROM concentration; however, in contrast to previous studies, the relationship between elevated pyridinium compound concentrations (and subsequent increases in solution viscosities) and conductivities of all solutions showed an approximately linear relationship up to the solubility limits of each species. The elevated concentrations that compound **17** could be assessed at, due to higher solubility, begins to show a plateau in conductivity, possibly corresponding to the influence of elevated viscosity having a dominant effect compared to the increased concentration of ions. Additionally, the maximum conductivities observed are 30.0 mS cm^{-1}, 25.0 mS cm^{-1}, and 32.8 mS cm^{-1} for compounds **3**, **5,** and **17** respectively. Notably, the conductivities observed for compounds **3**, **5**, and **17** in pure acetonitrile are surprisingly comparable to that of conductivities reported for solutions of acetonitrile with catholyte (i.e., TEMPO) and 0.1 to 1.5 M $TBAPF_6$, where reported conductivities range from 7.1 to a maximum of 26.8 mS cm^{-1}.[22] These results suggest that to achieve similar solution conductivities, the pyridiniums solutions near their solubility limit may not require nearly as much supporting electrolyte, as an inert salt typically introduced to solution as a mechanism to increase solution conductivities. The paired result of increasing conductivities with elevated viscosities, as these compounds approach their solubility limits in acetonitrile, is remarkably encouraging and further promotes 2,6-dimethylpyridiniums as a promising class of anolytes.

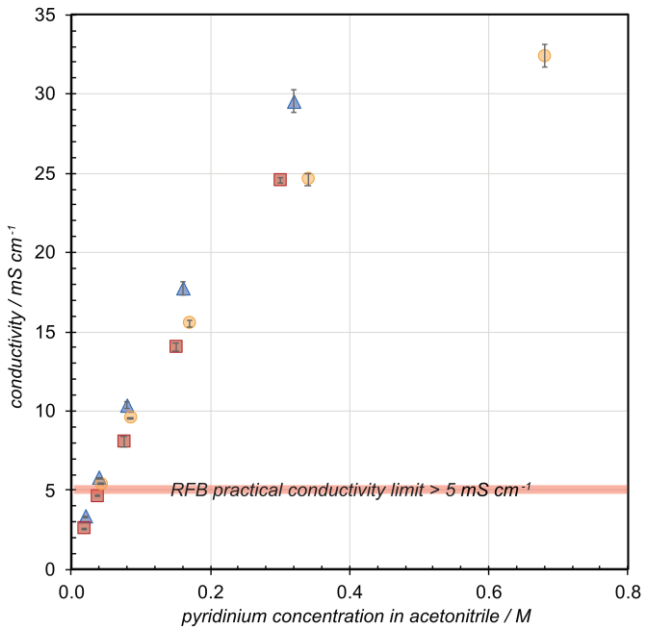

Figure 6. Concentration dependent conductivities in acetonitrile of compound **3** (blue triangles), **5** (red squares), and **17** (yellow circles) pyridiniums. Reported conductivity values represent the average of n = 3 replicates, and the error bars represent the respective standard deviations at (17.7 °C ± 0.5 °C).

CONCLUSIONS

In conclusion we have assessed primary electrochemical properties and subsequent physicochemical properties critical in the development of 2,6-dimethylpyridiniums as a potential anolyte for application in organic non-aqueous redox flow batteries. We assessed 23 derivatives of 2,6-dimethylpyridiniums featuring structural variations in the 4-position and N-position. Redox potential was found to be predictably influenced by the electronic nature of the substituents at the 4-position and N-position combined; however, some deviation was observed when sterics at the 4-position cause divergence between the planes of the pyridinium ring and 4-aryl ring. Diffusivities in the low concentration regime were adequately predicted by the Stokes-Einstein equation with a few notable exceptions, which may indicate that there is significantly less friction between solvent and solute than would be expected for organic salts in acetonitrile. Notably, we observe a limited effect on solution viscosities for three selected pyridiniums (compounds **3**, **5**,

and **17**), which will minimize the energy requirements pumping RFB solutions as well as improve the mass-transfer mechanisms occurring in solution. Additionally, the corresponding conductivities of compound **3**, **5**, and **17** in pure acetonitrile near their solubility limits are comparable to solutions containing high concentrations of common non-aqueous supporting electrolyte, which may have implications in the formulation of pyridinium based RFB solutions. Overall, this library of 2,6-dimethylpyridiniums demonstrates robust electrochemistry, practical viscosities, and high conductivities in acetonitrile that further promote their candidacy as an anolyte for organic non-aqueous energy storage applications.

ASSOCIATED CONTENT

Supporting Information. The following files are available free of charge. Synthesis procedures for pyriylium intermediates and pyridiniums, electrochemical characterization procedures, Hammett constants, diffusion coefficient calculations from crystal structure and CV analysis, conductivity, kinematic and dynamic viscosity measurements for **3**, **5**, and **17**.

AUTHOR INFORMATION

Corresponding Author

*David P. Hickey – hickeyd6@msu.edu

Author Contributions

S.S. and D.P.H. were responsible for the conceptualization of the project. A.L.P. performed all synthetic procedures. S.S. performed all viscosity measurements and electrochemical calculations. S.S. and D.S. performed all electrochemical measurements. W.R.K. and D.D.C. measured all conductivities. S.S. and D.P.H analyzed and interpreted the experimental and

computational data. S.S. and D.P.H. prepared the Supporting Information. S.S. and D.P.H. drafted the original version of the manuscript. All authors contributed to reviewing and editing the final manuscript. The manuscript was written through contributions of all authors. All authors have given approval to the final version of the manuscript.

ACKNOWLEDGMENT

The authors would like to thank S. Minteer for donating an Ubbelohde viscometer for this work.

REFERENCES

(1) Li, Z.; Jiang, T.; Ali, M.; Wu, C.; Chen, W. Recent Progress in Organic Species for Redox Flow Batteries. *Energy Storage Mater* **2022**, *50* (April), 105–138. https://doi.org/10.1016/j.ensm.2022.04.038.

(2) Chen, H.; Cong, G.; Lu, Y. C. Recent Progress in Organic Redox Flow Batteries: Active Materials, Electrolytes and Membranes. *Journal of Energy Chemistry* **2018**, *27* (5), 1304–1325. https://doi.org/10.1016/j.jechem.2018.02.009.

(3) Leung, P.; Li, X.; Ponce De León, C.; Berlouis, L.; Low, C. T. J.; Walsh, F. C. Progress in Redox Flow Batteries, Remaining Challenges and Their Applications in Energy Storage. *RSC Adv* **2012**, *2* (27), 10125–10156. https://doi.org/10.1039/c2ra21342g.

(4) Li, M.; Rhodes, Z.; Cabrera-Pardo, J. R.; Minteer, S. D. Recent Advancements in Rational Design of Non-Aqueous Organic Redox Flow Batteries. *Sustain Energy Fuels* **2020**, *4* (9), 4370–4389. https://doi.org/10.1039/d0se00800a.

(5) Darling, R. M. Techno-Economic Analyses of Several Redox Flow Batteries Using Levelized Cost of Energy Storage. *Curr Opin Chem Eng* **2022**, *37*, 100855. https://doi.org/10.1016/j.coche.2022.100855.

(6) Darling, R. M.; Gallagher, K. G.; Kowalski, J. A.; Ha, S.; Brushett, F. R. Pathways to Low-Cost Electrochemical Energy Storage: A Comparison of Aqueous and Nonaqueous Flow Batteries. *Energy Environ Sci* **2014**, *7* (11), 3459–3477. https://doi.org/10.1039/C4EE02158D.

(7) Zhang, J.; Corman, R. E.; Schuh, J. K.; Ewoldt, R. H.; Shkrob, I. A.; Zhang, L. Solution Properties and Practical Limits of Concentrated Electrolytes for Nonaqueous Redox Flow Batteries. *The Journal of Physical Chemistry C* **2018**, *122* (15), 8159–8172. https://doi.org/10.1021/acs.jpcc.8b02009.

(8) Li, M.; Case, J.; Minteer, S. D. Bipolar Redox-Active Molecules in Non-Aqueous Organic Redox Flow Batteries: Status and Challenges. *ChemElectroChem* **2021**, *8* (7), 1215–1232. https://doi.org/10.1002/CELC.202001584.

(9) Kosswattaarachchi, A. M.; Cook, T. R. Concentration-Dependent Charge-Discharge Characteristics of Non-Aqueous Redox Flow Battery Electrolyte Combinations. *Electrochim Acta* **2018**, *261*, 296–306. https://doi.org/10.1016/j.electacta.2017.12.131.

(10) Barton, J. L.; Milshtein, J. D.; Hinricher, J. J.; Brushett, F. R. Quantifying the Impact of Viscosity on Mass-Transfer Coefficients in Redox Flow Batteries. *J Power Sources* **2018**, *399*, 133–143. https://doi.org/10.1016/J.JPOWSOUR.2018.07.046.

(11) Samaroo, S.; Hengesbach, C.; Bruggeman, C.; Carducci, N. G. G.; Mtemeri, L.; Staples, R. J.; Guarr, T.; Hickey, D. P. C–H···π Interactions Disrupt Electrostatic Interactions between Non-Aqueous Electrolytes to Increase Solubility. *Nat Chem* **2023**, 1–9. https://doi.org/10.1038/s41557-023-01291-1.

(12) Attanayake, N. H.; Kowalski, J. A.; Greco, K. V.; Casselman, M. D.; Milshtein, J. D.; Chapman, S. J.; Parkin, S. R.; Brushett, F. R.; Odom, S. A. Tailoring Two-Electron-Donating Phenothiazines to Enable High-Concentration Redox Electrolytes for Use in Nonaqueous Redox Flow Batteries. *Chemistry of Materials* **2019**, *31* (12), 4353–4363. https://doi.org/10.1021/acs.chemmater.8b04770.

(13) Preet Kaur, A.; Neyhouse, B. J.; Shkrob, I. A.; Wang, Y.; Harsha Attanayake, N.; Kant Jha, R.; Wu, Q.; Zhang, L.; Ewoldt, R. H.; Brushett, F. R.; Odom, S. A. Concentration-Dependent Cycling of Phenothiazine-Based Electrolytes in Nonaqueous Redox Flow Cells. *Chem Asian J* **2023**, *18* (5). https://doi.org/10.1002/asia.202201171.

(14) Lall-Ramnarine, S. I.; Zhao, M.; Rodriguez, C.; Fernandez, R.; Zmich, N.; Fernandez, E. D.; Dhiman, S. B.; Castner, E. W.; Wishart, J. F. Connecting Structural and Transport Properties of Ionic Liquids with Cationic Oligoether Chains. *J Electrochem Soc* **2017**, *164* (8), H5247–H5262. https://doi.org/10.1149/2.0371708jes.

(15) Gong, K.; Fang, Q.; Gu, S.; Li, S. F. Y.; Yan, Y. Nonaqueous Redox-Flow Batteries: Organic Solvents, Supporting Electrolytes, and Redox Pairs. *Energy Environ Sci* **2015**, *8* (12), 3515–3530. https://doi.org/10.1039/c5ee02341f.

(16) Robinson, S. G.; Yan, Y.; Hendriks, K. H.; Sanford, M. S.; Sigman, M. S. Developing a Predictive Solubility Model for Monomeric and Oligomeric Cyclopropenium-Based Flow Battery Catholytes. *J Am Chem Soc* **2019**, *141* (26), 10171–10176. https://doi.org/10.1021/jacs.9b04270.

(17) Chai, J.; Lashgari, A.; Wang, X.; Williams, C. K.; Jiang, J. "jimmy." All-PEGylated Redox-Active Metal-Free Organic Molecules in Non-Aqueous Redox Flow Battery. *J Mater Chem A Mater* **2020**, *8* (31), 15715–15724. https://doi.org/10.1039/D0TA02303E.

(18) Alotto, P.; Guarnieri, M.; Moro, F. Redox Flow Batteries for the Storage of Renewable Energy: A Review. *Renewable and Sustainable Energy Reviews* **2014**, *29*, 325–335. https://doi.org/10.1016/j.rser.2013.08.001.

(19) Iyer, V. A.; Schuh, J. K.; Montoto, E. C.; Pavan Nemani, V.; Qian, S.; Nagarjuna, G.; Rodríguez-López, J.; Ewoldt, R. H.; Smith, K. C. Assessing the Impact of Electrolyte Conductivity and Viscosity on the Reactor Cost and Pressure Drop of Redox-Active

Polymer Flow Batteries. *J Power Sources* **2017**, *361*, 334–344. https://doi.org/10.1016/j.jpowsour.2017.06.052.

(20) Zmpitas, J.; Gross, J. Modified Stokes-Einstein Equation for Molecular Self-Diffusion Based on Entropy Scaling. *Ind Eng Chem Res* **2021**, *60* (11), 4453–4459. https://doi.org/10.1021/ACS.IECR.0C06090/SUPPL_FILE/IE0C06090_SI_001.PDF.

(21) Gering, K. L. Prediction of Electrolyte Viscosity for Aqueous and Non-Aqueous Systems: Results from a Molecular Model Based on Ion Solvation and a Chemical Physics Framework. *Electrochim Acta* **2006**, *51* (15), 3125–3138. https://doi.org/10.1016/j.electacta.2005.09.011.

(22) Stumme, N.; Perera, A. S.; Horvath, A.; Ruhunage, S.; Duffy, D. H.; Koltonowski, E. M.; Tupper, J.; Dzierba, C.; McEndaffer, A. D.; Teague, C. M.; Risko, C.; Shaw, S. K. Probing Redox Properties of Extreme Concentrations Relevant for Nonaqueous Redox-Flow Batteries. *ACS Appl Energy Mater* **2022**. https://doi.org/10.1021/acsaem.2c03712.

(23) Gering, K. L. Prediction of Electrolyte Conductivity: Results from a Generalized Molecular Model Based on Ion Solvation and a Chemical Physics Framework. *Electrochim Acta* **2017**, *225*, 175–189. https://doi.org/10.1016/J.ELECTACTA.2016.12.083.

(24) DiMauro, E. F.; Kozlowski, M. C. Phosphabenzenes as Electron Withdrawing Phosphine Ligands in Catalysis. *J Chem Soc Perkin 1* **2002**, *2* (3), 439–444. https://doi.org/10.1039/b101454o.

(25) Yue, H.; Zhu, C.; Shen, L.; Geng, Q.; Hock, K. J.; Yuan, T.; Cavallo, L.; Rueping, M. Nickel-Catalyzed C–N Bond Activation: Activated Primary Amines as Alkylating Reagents in Reductive Cross-Coupling. *Chem Sci* **2019**, *10* (16), 4430–4435. https://doi.org/10.1039/C9SC00783K.

(26) Samaroo, S.; Hengesbach, C.; Bruggeman, C.; Carducci, N. G. G.; Mtemeri, L.; Staples, R. J.; Guarr, T.; Hickey, D. P. C–H···π Interactions Disrupt Electrostatic Interactions between Non-Aqueous Electrolytes to Increase Solubility. *Nat Chem* **2023**. https://doi.org/10.1038/s41557-023-01291-1.

(27) Elgrishi, N.; Rountree, K. J.; McCarthy, B. D.; Rountree, E. S.; Eisenhart, T. T.; Dempsey, J. L. A Practical Beginner's Guide to Cyclic Voltammetry. *J Chem Educ* **2018**, *95* (2), 197–206. https://doi.org/10.1021/acs.jchemed.7b00361.

(28) Er, S.; Suh, C.; Marshak, M. P.; Aspuru-Guzik, A. Computational Design of Molecules for an All-Quinone Redox Flow Battery. *Chem Sci* **2015**, *6* (2), 885–893. https://doi.org/10.1039/c4sc03030c.

(29) Wedege, K.; Drazevic, E.; Konya, D.; Bentien, A. Organic Redox Species in Aqueous Flow Batteries: Redox Potentials, Solubility and Chemical Stability Supplementary Information. *Nature Publishing Group* **2016**, No. December, 1–13.

(30) Hansch, C.; Leo, A.; Taft, R. W. A Survey of Hammett Substituent Constants and Resonance and Field Parameters. *Chem Rev* **1991**, *91* (2), 165–195. https://doi.org/10.1021/cr00002a004.

(31) Holbrey, J. D.; López-Martin, I.; Rothenberg, G.; Seddon, K. R.; Silvero, G.; Zheng, X. Desulfurisation of Oils Using Ionic Liquids: Selection of Cationic and Anionic Components to Enhance Extraction Efficiency. *Green Chemistry* **2008**, *10* (1), 87–92. https://doi.org/10.1039/b710651c.

(32) Verdía, P.; Hernaiz, M.; González, E. J.; Macedo, E. A.; Salgado, J.; Tojo, E. Effect of the Number, Position and Length of Alkyl Chains on the Physical Properties of Polysubstituted Pyridinium Ionic Liquids. *Journal of Chemical Thermodynamics* **2014**, *69*, 19–26. https://doi.org/10.1016/j.jct.2013.09.028.

(33) Bandrés, I.; Alcalde, R.; Lafuente, C.; Atilhan, M.; Aparicio, S. On the Viscosity of Pyridinium Based Ionic Liquids: An Experimental and Computational Study. *Journal of Physical Chemistry B* **2011**, *115* (43), 12499–12513. https://doi.org/10.1021/jp203433u.

For Table of Contents Only